


# Capillary flow-driven blood plasma separation and on-chip analyte detection in microfluidic devices

M. Sneha Maria<sup>1,2</sup> · T. S. Chandra<sup>2</sup> · A. K. Sen<sup>1</sup> 

Received: 20 November 2016 / Accepted: 22 March 2017 / Published online: 30 March 2017  
© Springer-Verlag Berlin Heidelberg 2017

**Abstract** We report a comprehensive review on the capillary flow-driven blood plasma separation and on-chip analyte detection in microfluidic devices. Blood plasma separation is the primary sample preparation step prior to most biochemical assays. Conventionally, centrifugation is used for the sample preparation process. There are numerous works reporting blood plasma separation in microfluidic devices which aim at miniaturizing the sample preparation procedure. Capillary-based blood plasma separation shows promise in actualizing point-of-care diagnostic devices for applications in resource-limited settings including military camps and rural areas. In this review, the devices have been categorized based on active and passive plasma separation techniques used for the separation of plasma from capillary-driven blood sample. A comparison between different techniques used for blood plasma separation is outlined. On-chip detection of analytes present in the separated plasma obtained using some of these reported devices is also presented and discussed.

## 1 Introduction

Microfluidics, the science and technology that manipulates fluids in channels with dimensions tens to hundreds of micrometres, enables the miniaturization of several biological and chemical processes (Whitesides 2006). Significant

research works have been carried out to shrink a laboratory onto a chip, i.e. lab on chip, which executes the laboratory protocol within itself for an analysis (Juncker 2002). Microfluidic systems have been designed and fabricated for a number of applications in medicine, biology, physics and chemistry (Whitesides 2006). In general, microfluidic devices drive, mix, separate and process different working fluids in a network of microchannels. Such manipulations including the injection and removal of fluids are carried out either using active or passive mechanisms. Active microfluidic devices use external energy for driving and manipulating fluids using pumps and valves while passive devices work autonomously without the aid of external energy. Most microfluidic systems are active and rely on external macroscopic peripherals such as pumps and other energy sources for fluid manipulation thus making it difficult to realize fully autonomous standalone lab-on-chip devices.

One important class of passive microfluidic devices utilizes the principle of capillary flow for fluid manipulation. Capillary flow microfluidics have greater attraction since such devices are self-contained and autonomous, bringing down the cost as well as the fabrication and device complexity. Capillary flow devices can replace pumps and valves that are required for driving fluid into the device thus minimizing interference with other modules. In such devices, flow can be interactively controlled and synchronized as required by controlling the meniscus pressure inside the channels (Juncker 2002). Due to such distinctive advantages, capillary-based microfluidic devices have been adopted by life science industries since more than three decades (Juncker 2002; Manz et al. 1990). The commercially available diagnostic devices are mostly lateral flow-based immune-chromatographic test strips that are made of porous substrates (Swiss Precision Diagnostics GmbH 1985) which generate strong capillary action for the flow of buffers, antigens and antibodies for detection.

---

✉ A. K. Sen  
ashis@iitm.ac.in

<sup>1</sup> Department of Mechanical Engineering, Indian Institute of Technology Madras, Chennai 600036, India

<sup>2</sup> Department of Biotechnology, Indian Institute of Technology Madras, Chennai 600036, India

Diagnostic tests are performed to confirm the presence or absence of a disease in a symptomatic individual or screen for disease in an asymptomatic individual. Such tests also provide prognostic information in patients with established disease and monitor therapy with its benefits and side effects (Abram 2015). It has been estimated that diagnostic tests inform approximately seventy per cent of medical decisions (AdvaMed 2012). Blood diagnostic tests are the most common primary tests recommended by doctors although not conclusive. Types of blood tests include complete blood count (red blood cells (RBCs), white blood cells (WBCs), platelets, haemoglobin, haematocrit, mean corpuscular volume), blood chemistry tests, blood enzyme tests and blood tests to assess heart disease risk (National Heart, Lung and Blood Institute 2012). Haematocrit is the volume percentage (%) of red blood cells in blood. The complete blood count can help diagnose anaemia, infections, clotting problems, blood cancers and immune system disorders. The blood chemistry tests can give information about muscles (including the heart), bones and organs, such as the kidneys and liver. The basic metabolic panel includes blood glucose, calcium and electrolyte tests, as well as blood tests that measure kidney function. Blood enzyme tests help us to analyse specific activity of enzymes in our body including creatine phosphokinase, heart enzymes and liver enzymes (Pietrangelo 2015). Monitoring the rise or fall of enzyme levels can aid in the diagnosis of a variety of conditions from a disease to a simple muscle strain. The blood lipoprotein panel (total cholesterol, low-density lipoprotein (LDL or bad cholesterol), high-density cholesterol (HDL or good cholesterol) and triglycerides) can signal the risk of coronary heart disease (CHD) (see footnote 4). Therefore, blood diagnostic tests can be used to assess general state of health of an individual.

Such tests could potentially benefit from the field of microfluidics. According to Toner and Irimia (Toner and Irimia 2005), bringing an entire blood analysis laboratory to the bedside (home or doctor's office) is poised to reshape the delivery of health care as it would allow for rapid and accurate diagnosis and prognosis. However, most of the blood tests are performed on plasma, the liquid component of blood and source of indicators of many diseases, which constitutes 54.3% of the blood sample. Separation of plasma from the interfering blood cells, termed 'plasmapheresis', is the most essential sample preparation step prior to further biochemical analysis and will increase assay sensitivity and reliability (Kovarik et al. 2012; Dimov et al. 2011). In contrast to centrifugation, the conventional method of plasma separation, microfluidic technology requires very low sample volume and enables easier integration with the detection modules. On-chip blood sample preparation would lead to more gentle, fast and consistent manipulation of living cells, and therefore more accurate and better quality of data (Toner and

Irimia 2005). Furthermore, the point-of-care diagnostic tests will be simpler and can overcome the difficulties with sample handling, transportation and storage enabling commercialization and public access to point-of-care devices (Kovarik et al. 2012; Kersaudy-Kerhoas and Sollier 2013).

There has been a lot of effort towards miniaturizing blood plasma separation in concordance with its importance (Kersaudy-Kerhoas and Sollier 2013; Hou et al. 2011; Mukherjee et al. 2009; Tripathi et al. 2015). The process of plasma separation can be classified into two categories: active and passive methods. Active methods of plasma separation yield higher volume of plasma by employing electric, magnetic and acoustic energy but have limitations in terms of simplicity, ease of use, portability and cost. On the other hand, passive techniques are easy to use, simpler, gentler to cells and cost-effective. In this technique, filters (Crowley and Pizziconi 2005; Aran et al. 2011), micro-channel bend structures (Maria et al. 2015; Blatter et al. 2004; Faivre et al. 2006) or microposts (Davis et al. 2006) are used to achieve plasma separation by exploiting the inherent properties of the fluid and the suspended particles. Nevertheless, the aforesaid devices are active microfluidic systems and require external pressure sources, i.e. pumps, for driving the sample fluid into the device. Hence, these devices may still be constrained by challenges in terms of fabrication and operation (Kim et al. 2010). Therefore, the use of active microfluidic blood plasma separation devices in point-of-care testing becomes limited. It is more desirable to have an autonomous blood plasma separator for integration with lab-on-chip platforms for regular tests on patients at the bedside. Self-infusion of sample by capillary effect will bring down the complexity, size and cost of the device significantly (Maria et al. 2016). However, not many reports are available on capillary-based plasma separation devices. In the present review, the development of various capillary-based blood separation devices is reported, and the working principle, design and applications are discussed.

## 2 Capillary-driven blood plasma separation: passive techniques

Several attempts have been made to develop fully autonomous blood plasma separation devices that use passive techniques to separate plasma from self-infused blood sample. Passive techniques including conventional filtration (Son et al. 2014; Wu et al. 2012) and sedimentation were exploited for achieving plasma separation (Dimov et al. 2011; Son et al. 2014; Kuroda et al. 2014; Maria et al. 2017; Park et al. 2016). In addition to cross-flow filtration with the help of shallow channels (Kim et al. 2010; Khumuang et al. 2007; Sakamoto et al. 2012) and microposts

(Park et al. 2016; Madadi et al. 2015), self-built-in filter made of RBCs have also been reported (Maria et al. 2016, 2017; Lee and Ahn 2013). The self-infusion of sample has been enabled by either use of hydrophilic substrates (Wu et al. 2012; Park et al. 2016; Khumpuang et al. 2007), degassing of the PDMS microchannels (Dimov et al. 2011; Son et al. 2014; Kuroda et al. 2014) or modifying the substrate with surfactant (Kim et al. 2010; Madadi et al. 2015), silica nanobead coating (Lee and Ahn 2013) and oxygen plasma treatment (Maria et al. 2016; Wu et al. 2012; Maria et al. 2017; Sakamoto et al. 2012).

In capillary flows through a microchannel, the driving force is the pressure drop across the microchannel which can be described by the Young–Laplace equation as follows (Laplace 1829),

$$\Delta P = \sigma \cos \theta \left( \frac{1}{h} + \frac{1}{w} \right) \tag{1}$$

where  $\sigma$  is the surface tension of the fluid,  $\theta$  is the contact angle of the fluid with the channel wall,  $h$  is the half-height and  $w$  is the half-width of the rectangular microchannel.

### 2.1 Actuation by degassing of channels

Dimov et al. (2011), Son et al. (2014) and Kuroda et al. (2014) have used degassing of PDMS for creating the capillary force required to drive the flow into a microchannel device. When the air present in the channel walls is evacuated through the channels and inlet reservoirs, the pumping energy is stored in the bulk PDMS during the degassing. When the PDMS is returned to atmosphere, the direction of air transfer is reversed. When the samples are introduced at the inlets, it starts flowing into the channels as the dissolution of air into PDMS reduces the pressure inside the channels and the outlet. The characterization of flow rate in a degassed channel is reported by Hosokawa et al. (2004). The flow rate was found to be insensitive to the degassing time,  $t_d$ , but was largely affected by the idling time (the time from the ventilation of the vacuum desiccator to the completion of the liquid dispensing),  $t_i$  due to the inactivation of PDMS by re-dissolution of air from the atmosphere. The flow rate of the liquids into the microchannel  $q$  at idling time  $t_i$  is expressed as,

$$q \sim \frac{2AD(C_1 - C_0)}{l} \exp(-t_i/\tau) \tag{2}$$

where  $A$  is the area of the outlet reservoir wall,  $D$  is the diffusion coefficient of air in PDMS,  $C_1$  is the boundary air concentration,  $C_0$  is the equilibrium air concentration in the degassing step,  $l$  is half of PDMS wall thickness and time constant  $\tau = (4/\pi^2)(l^2/D)$ .

The standalone self-powered integrated microfluidic blood analysis system (SIMBAS) developed by Dimov

et al. (2011) used an integrated trench to capture and trap RBCs and WBCs by sedimentation as shown in Fig. 1a. In addition, the top slide was manually coated with a hydrophobic pen only on the region that overlaps the filter trench, to prevent blood cells from flowing past the filter trench. The capture efficiency of the filter trench was simulated by considering the relevant forces. In the trench, the forces acting on the RBCs are the buoyancy-corrected gravitational sedimentation force  $F_{gb} = \Delta m_p g$  and the fluid drag force  $F_d$ , where  $\Delta m_p$  is the difference between the masses of the cell and the displaced fluid and  $g$  is gravitational acceleration. The trajectories of the cells were obtained from the force balance equation

$$m_p \frac{d^2 r}{dt^2} = F_d \left( t, r, \frac{dr}{dt} \right) + F_{gb} \tag{3}$$

where  $t$  is the time,  $r$  is the position vector of the particle. The expression for the drag force  $F_d$  is given as (Coulson et al. 1991),

$$|F_d| = \pi r_p^2 \rho (|v - v_p|)^2 \left( 1.84 \text{Re}_p^{-0.31} + 0.293 \text{Re}_p^{0.06} \right)^{3.45},$$

$$\text{Re}_p = \frac{(|v - v_p| 2r_p \rho)}{\eta} \tag{4}$$

where  $m_p$ ,  $r_p$  and  $v_p$  are the mass, radius and velocity of the suspended spherical particle, respectively,  $\rho$ ,  $\eta$  and  $v$  are the density, dynamic viscosity and velocity of the fluid and  $\text{Re}_p$  is the particle Reynolds number. The simulation results showed that 100% capture efficiency can be achieved when the normalized length and depth of the trench (with the height of the inlet channel) becomes  $>5$  and the velocity  $\leq 90$  mm/s. The device was made of PDMS and activated by maintaining it in a low-pressure ( $<0.3$  atm) condition for at least 15 min ( $t_d$ ), and the sample blood was introduced at the inlet within 2.0 min ( $t_i$ ) after removing it from the vacuum. Separation of plasma from 5  $\mu\text{l}$  of whole blood was achieved within 10 min, and purification efficiency of  $>99\%$  was found.

A similar blood plasma separation device actuated by degassing was reported by Son et al. (2014) in which a membrane filter on top of a vertical up-flow chamber was used to separate plasma by filtration as shown in Fig. 1b. The gravitational force competes with the fluidic drag to pull the blood cells towards the bottom of the chamber and thus prevents clogging of the filter and reduces haemolysis. The device was optimized with the help of an analytical model that was derived assuming that the vertical flow of single RBC is under the influence of gravitational and drag forces as follows,

$$F_T = F_D - F_g = \alpha \cdot (v_{\text{fluid}} - v_{\text{cell}}) - mg \tag{5}$$

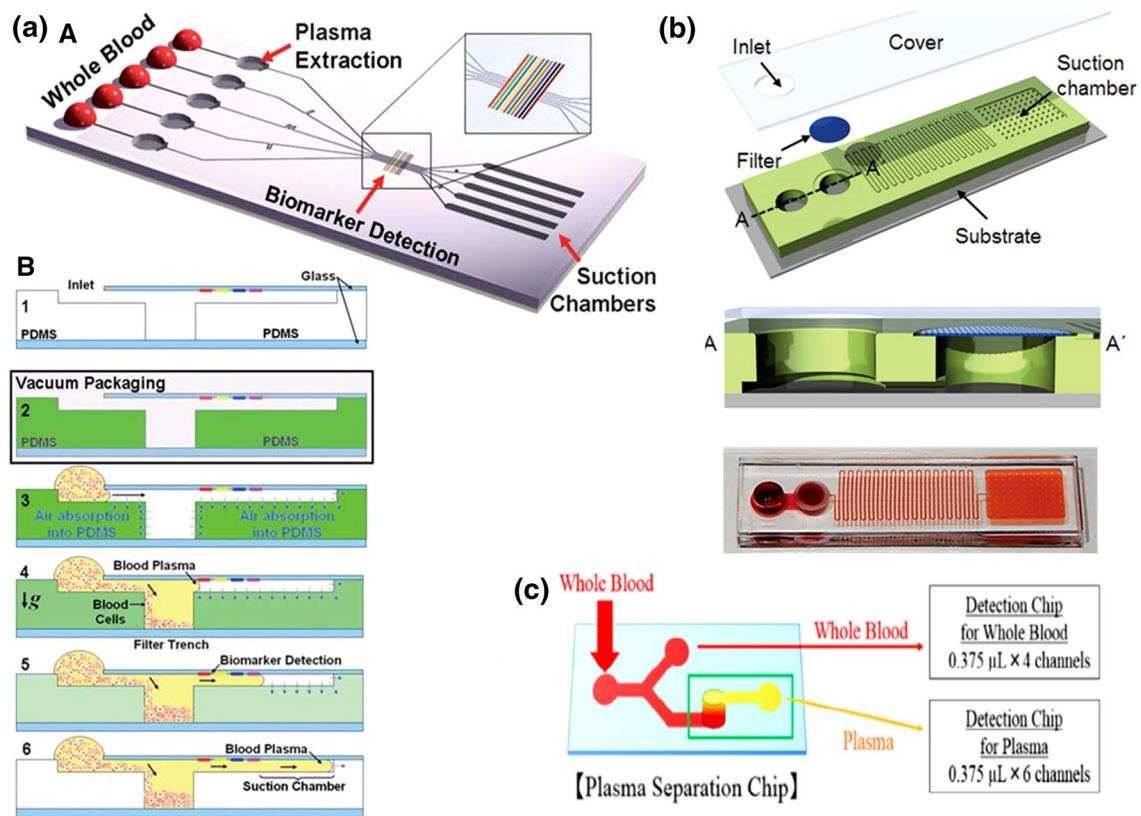


**Fig. 1** Images showing microfluidic devices in which the actuation of sample is achieved by degassing and separation of plasma is obtained by sedimentation. **a** Sedimentation in filter trenches (Dimov

et al. 2011), **b** sedimentation and filtration in a chamber with membrane on top (Son et al. 2014), **c** sedimentation in a vertical up-flow chamber (Kuroda et al. 2014)

$$v_{\text{cell}} = v_{\text{fluid}} - \frac{mg}{\alpha} \quad (6)$$

where  $F_T$  is the total force on the cell,  $F_D$  is the fluidic drag force,  $F_g$  is the gravitational force,  $\alpha$  is the drag coefficient,  $v_{\text{fluid}}$  is the fluid velocity,  $v_{\text{cell}}$  is the velocity of the cell and  $m$  is the mass of the cell. Initially, when  $v_{\text{cell}} > 0$  the cells move upward in the up-flow chamber and when  $v_{\text{cell}} < 0$ , the RBCs will move downward. The device design ensures that  $v_{\text{fluid}}$  varies between higher and lower values since the initial high velocity decreases the time required to fill up the chamber and increases the plasma volume separated by the filter. On the other hand, lower velocity facilitates sedimentation and thus separation of plasma.

When the sample reaches the filter, the fluid velocity is reduced due to the filter resistance. The accumulation of RBCs beneath the filter increases the filter resistance and decreases the fluid velocity further and results in the sedimentation of RBCs in the chamber under the influence of gravitational force. Using whole blood sample, 2.4  $\mu\text{l}$  of plasma (20% plasma recovery) was separated in 20 min and the plasma volume increases further with time.

Kuroda et al. (2014) used evacuation of channels by degassing in a vacuum desiccator (20 min) for driving the blood sample into the device. Blood sample of 10% haematocrit was added to the inlet within 2 min ( $t_i$ ) after removal from the vacuum. Sedimentation of blood cells and ascension of plasma in a cylindrical channel as shown in Fig. 1c was observed after 20 min. Assuming the blood cells as hard spheres sinking freely through plasma (uniform medium), the erythrocyte sedimentation rate (ESR) was derived from the Stokes equation and given as,

$$v_{\text{blood}} = (2/9)(\rho_s - \rho)gR_e^2\phi(H)/f\eta \quad (7)$$

where  $\rho_s$ ,  $\rho$  and  $\eta$  are the average density of RBC, density and viscosity of the suspension of blood cells, respectively.  $R_e$  and  $H$  are, respectively, the effective radius and volume fraction, and  $\phi(H)$  and  $f$  are parameters to compensate for the effect of density and deformability. Degas-driven blood plasma separation techniques reported by Dimov et al. (2011), Son et al. (2014) and Kuroda et al. (2014) show high plasma recovery but require blood to be introduced at the inlet immediately (within 2.0 min) after removal of the device from vacuum desiccator. Although vacuum desiccator can be mimicked by a vacuum pouch, the quality of the



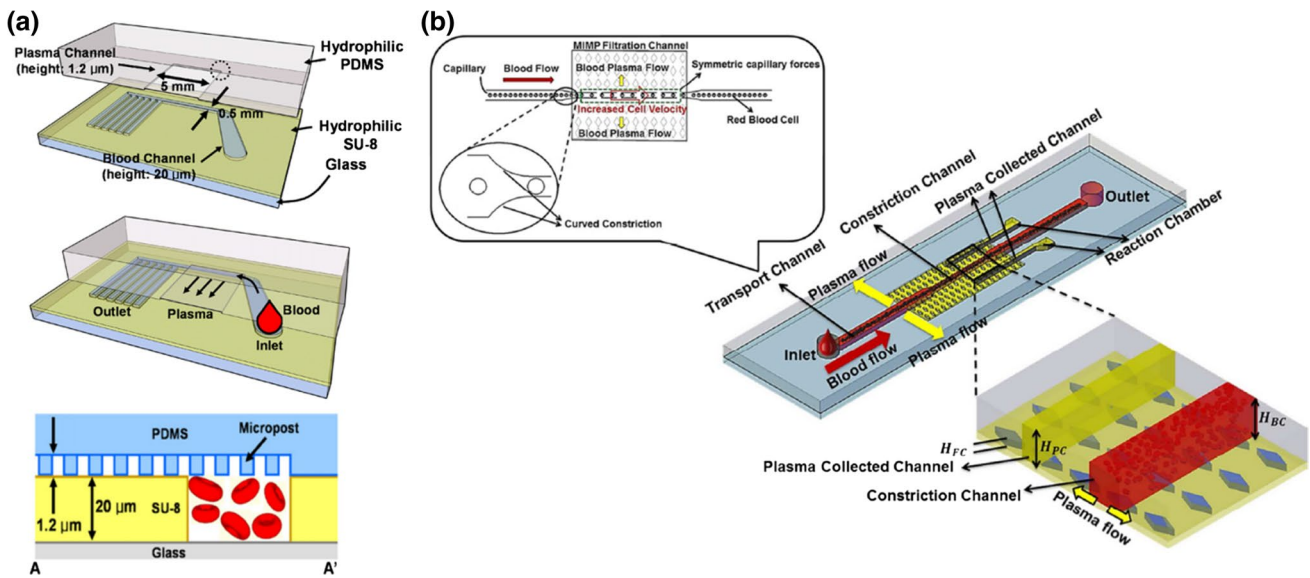


**Fig. 2** Images showing microfluidic devices where the actuation is achieved by surfactant-modified PDMS and plasma extraction is obtained by a planar cross-flow filtration through shallow channels (Kim et al. 2010) and **b** filtration by diamond micropost arrays (Madadi et al. 2015)

vacuum and the idling time,  $t_i$ , are critical and could significantly affect the performance of the device.

### 2.2 Actuation by surfactant-modified PDMS

Kim et al. (2010) reported plasma separation without the use of external energy. In this work, non-ionic surfactant (Silwet L-77) was mixed with PDMS to make it hydrophilic. The spreading coefficient  $S$  is expressed as,

$$S = \sigma_{SG} - \sigma_{LG} - \sigma_{SL} \tag{8}$$

where  $\sigma_{SG}$ ,  $\sigma_{LG}$  and  $\sigma_{SL}$  are the interfacial tensions between solid and gas, liquid and gas, solid and liquid, respectively. Use of Silwet L-77 reduces the interfacial tension of both solid–liquid and liquid–gas interfaces, and the spreading coefficient increases giving rise to the spreading of aqueous solutions on the PDMS surface. Additionally, the surfactant-modified PDMS surfaces are also less susceptible to biofouling.

The hydrophilic PDMS and SU8 microstructures drive the flow of blood into the device from the inlet. As shown in Fig. 2a, the device is of two layers. SU8 patterned glass slide with 20- $\mu$ m channel is used as the bottom layer for the transportation of blood. The top hydrophilic PDMS layer has channels of 1.2  $\mu$ m height for separating plasma from blood in the bottom channel by cross-flow filtration. Here, the capillary pressure of the fluid meniscus in the rectangular channel is given by,

$$P_c = -\gamma \left( \frac{\cos \theta_b + \cos \theta_t}{h} + \frac{\cos \theta_l + \cos \theta_r}{w} \right) \tag{9}$$

where  $\gamma$  is the surface tension of the fluid,  $\theta_b$ ,  $\theta_t$ ,  $\theta_l$  and  $\theta_r$  are the contact angles of the fluid at the bottom, top, left and right walls, respectively and  $h$  and  $w$  are the height and width of the microchannel. Using the reduced-order model based on momentum conservation, the passive capillary filling rate,  $u$ , and position of the free surface front,  $L$ , are given as,

$$u = \frac{A(1 - e^{-Bt})}{2BL}, L = \left[ \frac{A}{B^2} e^{-Bt} + \frac{At}{B} + \left( L_0^2 - \frac{A}{B^2} \right) \right]^{1/2} \tag{10}$$

where  $A = \frac{4\gamma \cos \theta}{\rho h}$ ,  $B = \frac{12\mu}{\rho h^2}$ ,  $t$  is the time instants during the filling process,  $L_0$  is the initial microchannel length that the liquid hold at zero velocity,  $\rho$  is the fluid density,  $\mu$  is the dynamic viscous coefficient,  $\gamma$  is the surface tension coefficient,  $\theta$  is the contact angle, and  $h$  is the height of the microchannel.

Though the purification efficiency was 100%, the plasma recovery was found to be very low due to the shallow plasma channels resulting in very high resistance. Only 20 nl of plasma was obtained from 10  $\mu$ l of whole blood sample. However, the above work provided the evidence for capillary-driven flow with surfactant-added PDMS, based on which Madadi et al. (2015) built a device which could separate 0.1  $\mu$ l of plasma from 5  $\mu$ l of blood in 3–5 min. In the device, the top layer is surfactant-added PDMS and the bottom layer is an etched glass slide. The device consists of three consecutive channels, the transport channel, constriction channel and plasma collection channel, as shown in Fig. 2b. A filtration chamber composed of diamond micropost arrays on either side of the constriction

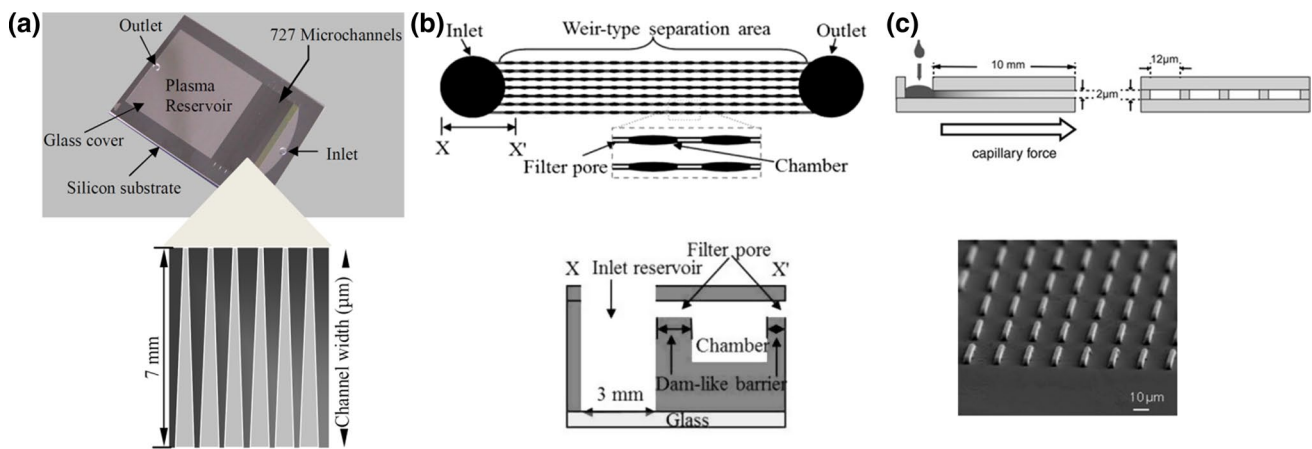


**Fig. 3** Images showing microfluidic devices with **a** glass and silicon substrates for capillary flow and tapering microchannels for plasma extraction (Khumpuang et al. 2007), **b** glass substrate and pore structures for capillary flow and weir-type PDMS microfilter for plasma

extraction (Wu et al. 2012), **c** oxygen-irradiated and poly-L-Lysine-coated PMMA channels for actuation and array of shallow channels for plasma separation (Sakamoto et al. 2012)

channel etched on glass was used to decrease the flow rate resistance  $R_F$  and increase capillary force so as to increase the plasma volume. This flow resistance  $R_F$  is calculated as follows,

$$R_F = \frac{12\mu L}{wH^3} \left( \frac{1}{2\varepsilon - 1} \right) \quad (11)$$

where  $\mu$  is the fluid viscosity,  $L$  is the length of the microchannel,  $w$  is the half-width of the microchannel,  $H$  is the half-height of the microchannel and  $\varepsilon$  is the porosity. Further, the constriction channel following the transport channel helps in preventing RBC clogging by imparting local flow acceleration on the cells. The plasma which gets filled in the filtration channel (of 2  $\mu\text{m}$  height) gets collected in the plasma collection channel which is as high as the transport channel (of 10  $\mu\text{m}$  height). Using this device, the plasma purification efficiency was measured to be 98%.

### 2.3 Actuation by hydrophilic substrates

The use of naturally hydrophilic substrates, e.g. glass and silicon, also facilitates in driving fluid by capillary action on account of its wettability. Khumpuang et al. (2007) experimented with silicon and glass for self-driven flow of sample blood. Tapering microchannels were etched on the silicon wafer to separate the blood cells from plasma, as shown in Fig. 3a. The flow rate was further increased by oxidization of silicon in a thermal oxidation furnace for deposition of a 40-nm-thick silicon dioxide layer to increase the hydrophilicity. Though the higher driving force was realized, desired plasma volume (1.0  $\mu\text{l}$ ) was not achieved. The nature of the separated plasma also indicated possible haemolysis or reduced purification efficiency.

Wu et al. (2012) developed a weir-type PDMS device microfilter to separate plasma by dead-end filtration as given in Fig. 3b. The device consists of an inlet, seven parallel microchannels and an outlet. Twenty-one equally spaced barriers were fabricated in each of the microchannels forming twenty 100- $\mu\text{m}$ -deep chambers with adjacent chambers connected by filter pores of 6  $\mu\text{m}$  height. While the chambers remove RBCs by sedimentation as the cascade of microstructures delay the flow, the pores are used for the hydrodynamic control of capillarity-driven fluid. Smaller pores and deeper chambers showed better blood plasma separation. The glass substrate and oxygen plasma-treated PDMS facilitates the capillary flow of blood into the device. Experiments were carried out within 10–45 min after oxygen plasma treatment, and the device was efficient with blood sample of haematocrit  $\leq 20\%$ .

The relatively low surface energy of PMMA has a negative effect on the adhesion of coating and biocompatibility and hence requires modifications to improve its wettability (Chai et al. 2004). Sakamoto et al. (2012) modified PMMA microchannels by oxygen irradiation followed by poly-L-Lysine coating to make the channels hydrophilic to drive the blood sample through the device. The oxygen plasma exposure introduces polar functional groups containing oxygen groups on the surface making it hydrophilic and also produces a negatively charged surface. PLL exhibited strong adsorption owing to the electrostatic interaction between the oxygen plasma-treated PMMA surface (negatively charged) and the PLL side residue (positively charged). The numerous active amino groups on PLL promote cell adhesion. It also offers good biocompatibility, a flexible molecular backbone and relatively good solubility in water. As shown in Fig. 3c, they have designed array of

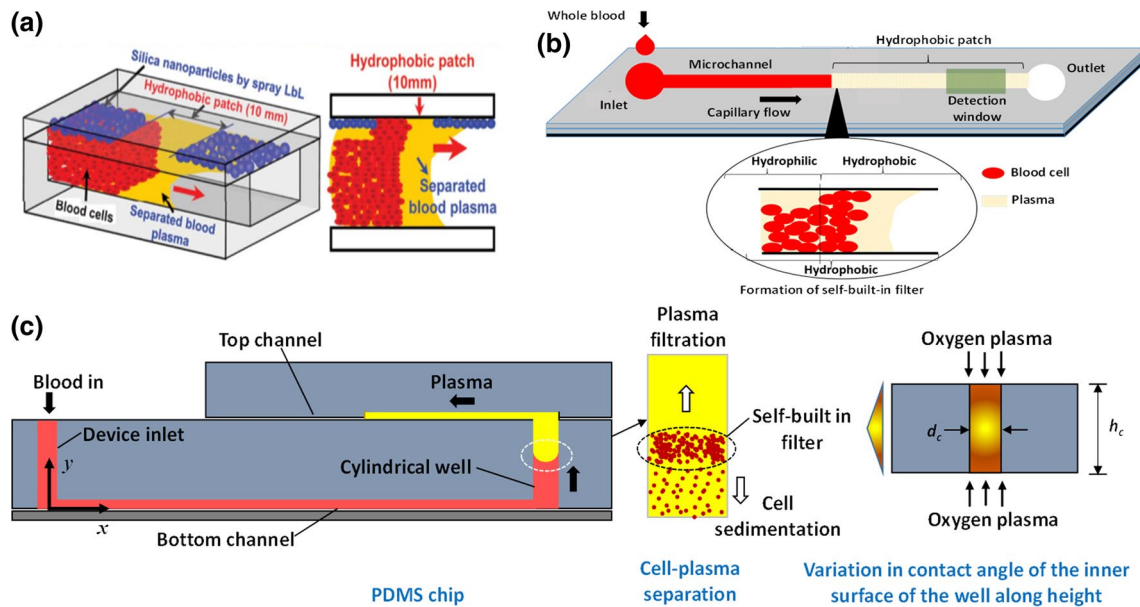


**Fig. 4** Images showing plasma separation in microfluidic devices with **a** silica nanobead-coated microchannel for actuation and plasma separation at the hydrophobic patch of devices (Lee and Ahn 2013), **b** oxygen plasma-treated microchannel for actuation and plasma

separation at the hydrophobic patch of devices (Maria et al. 2016), **c** oxygen plasma-treated microchannel for actuation and sedimentation effects for plasma separation (Maria et al. 2017)

channels of 2 μm depth in order to filter the red blood cells from whole blood. The experiments showed separation of 150 nl plasma from 20 μl of whole blood in 3 min with 99% purification efficiency.

## 2.4 Plasma separation using wetting contrast

### 2.4.1 Actuation by hydrophilic silica nanoassembly

Some research works have exploited the wetting contrast of hydrophilic and hydrophobic substrates to achieve plasma separation. Lee and Ahn (2013) used asymmetric capillary force generated by the sprayed silica nanobead multilayers in the microchannel and hydrophobic patch to achieve plasma separation, as shown in Fig. 4a. The COC substrate is treated with adhesion promoters followed by five layer by layer coating of patterned 12-nm silica nanobead structure to make the top surface superhydrophilic surfaces for driving the sample. The bottom and the side walls of the channel remain uncoated. A small portion of the top surface is not coated in order to create a hydrophobic patch inside the channel. The hydrophobic patch acts as a flow barrier causing the accumulation of the blood cells over the patch which forms a built-in microfilter. The plasma, having lower viscosity compared to the blood sample, flows past the hydrophobic patch and arrives at the superhydrophilic coating. Thus, strong asymmetric capillary effect developed in the channel is used for the blood plasma separation. The asymmetric capillary force  $F_{cas}$  induced by

the superhydrophilic coating and the hydrophobic patch is given as,

$$F_{cas} = 4\pi\gamma R(\cos\theta_{phi} - \cos\theta_{pho}) \approx 5.5(\cos\theta_{phi} - \cos\theta_{pho})(nN) \tag{12}$$

where  $\gamma$  is the surface tension of water at 20 °C (72.8 mJ/m<sup>2</sup>),  $R$  is the radius of the nanobead and  $\theta_{phi}$  and  $\theta_{pho}$  are the contact angles on the hydrophilic and hydrophobic surfaces, respectively. Using this device, 102 nl of plasma was separated from 3 μl of whole blood (6.8% plasma recovery) within 10 min. Though the use of silica nanoassembly makes the device fabrication very complicated and expensive, the phenomena of asymmetric capillary effect and self-built-in filter have inspired other similar plasma separation works as reported in the following section.

### 2.4.2 Actuation by oxygen plasma-treated PDMS

When PDMS surface is exposed to oxygen plasma, the surface chemical modifications on the surface increase the surface energy and thus increasing wettability of the surface and enabling flow. Silanol (-OH) groups are formed on the surface of PDMS on reaction with oxygen plasma (Bhattacharya et al. 2005). As the silanol groups are polar in nature, the PDMS surface becomes highly hydrophilic and the advancing contact angle of deionized water significantly reduces. Further, when two

plasma-exposed surfaces (PDMS/glass) are brought into contact, the silanol groups condense with each other and yield Si–O–Si bonds which form the basis for irreversible bonds. The bond strength reduces when the contact is delayed or at very high exposure times due to formation of cracks. For successful and leak-proof bonding of two surfaces, right plasma exposure parameters are required which are discussed by Bhattacharya et al. (2005). A contact angle less than  $5^\circ$  is a general requirement for very high bond strength. Due to rapid recovery of hydrophobicity after exposure, there is negligible non-specific adsorption of biomolecules, i.e. proteins, DNA, on the PDMS surface compared to hydrophilic substrates such as silicon (Bhattacharya et al. 2010).

Maria et al. (2016) reported a fully autonomous, inexpensive device which consists of a simple straight rectangular PDMS microchannel bonded to a flat PDMS layer. In this work, the top PDMS channel was treated with oxygen plasma to render it hydrophilic for the self-infusion of blood into the channel from the inlet. The top PDMS layer, which forms the top and two side walls of the microchannel, is hydrophilic everywhere except the hydrophobic region while the bottom PDMS layer is hydrophobic throughout. Thus at the hydrophobic region, all four walls of the microchannel are hydrophobic. As in Lee and Ahn (2013), the self-infused blood sample halts at the hydrophobic region, due to large contact angles and small Young–Laplace pressure, and leads to the accumulation of blood cells near the region. The aggregated blood cells act as a self-built-in filter to facilitate the separation of plasma which flows downstream due to its lower viscosity, as shown in Fig. 4b. Using the device, 450 nl of plasma was separated from whole blood sample (22.5% plasma recovery) within 15 min. Also, it was found that the volume of plasma continues to increase with time. The hydrophobicity recovery of the PDMS was averted by incubation in water with or without vacuum. Thus, the device was also shown to work with same efficiency even after more than 2 weeks. The work also presents an expression for calculating the average velocity  $u_{\text{avg}}$  of a capillary meniscus along the length of a channel with hydrophilic walls on all four sides. Assuming non-Newtonian flow (Casson model) and infinite parallel plate, the theoretical model is described as,

$$u_{\text{avg}} = \frac{1}{k_1} \left( k_0 h + \frac{P_0}{x} \frac{h^2}{12} \right) \quad (13)$$

where  $k_0 = 0.004$  Pa,  $k_1 = \eta_p (1 + 0.025 H + 7.35 \times 10^{-4} H^2)$ ,  $P_0$  is the inlet pressure,  $x$  is the location along the length of the channel and  $h$  is the height of the channel.

Maria et al. (2017) report a sedimentation-based plasma separation from capillary-driven blood sample which also uses oxygen plasma-treated PDMS for the infusion of the sample blood. The blood flows through a straight channel

in the bottom layer and up into a vertical cylindrical well, as shown in Fig. 4c. In this device, the hydrophilicity gradient generated in the well of the PDMS device augments the sedimentation of blood cells and increases the plasma separated by the device which flows into the channel in the top layer. An expression for predicting the meniscus location of the non-Newtonian fluid along the straight capillary channel  $x(t)$  is developed, which is given as follows,

$$x(t) = \left[ \frac{n+1}{2(2n+1)} \left( \frac{\sigma \cos \theta}{m} \right)^{\frac{1}{n}} h \right]^{\frac{n}{n+1}} (t - t_0)^{\frac{n}{n+1}} \quad (14)$$

where  $m$  and  $n$  are constants that depend on the liquid properties,  $\sigma$  is surface tension of the liquid,  $\theta$  is the contact angle of the liquid with the channel wall and  $h$  is the height of the channel. Also, in a cylindrical well, the sedimentation velocity of RBCs in a blood of known cell concentration is reported as,

$$V = V_s \varepsilon^2 f(\varepsilon) \quad (15)$$

where  $\varepsilon$  is the liquid concentration,  $V_s$  is the Stokes velocity and  $V_s f(\varepsilon) = 0.1063 \varepsilon^{4.08}$  is a correlation developed from experimental data.

In this work, using a device with a well of 4.0 mm height and 1.0 mm diameter, 2.0  $\mu\text{l}$  of plasma was obtained (from  $<10$   $\mu\text{l}$  whole blood) in 15 min with a purification efficiency of 99.9%. The device was also shown to operate with same efficiency after 2 weeks following its incubation in water under vacuum.

The use of oxygen plasma to create hydrophilic PDMS demonstrated in the above two works (Maria et al. 2016, 2017) makes the device fabrication simpler and less expensive as compared to the coating of silica nanoassembly over PDMS substrate (Lee and Ahn 2013). Also, the plasma recovery in the oxygen plasma-treated hydrophilic PDMS device (Maria et al. 2016, 2017) was found to be significantly higher as compared to the silica nanoassembly-based device (Lee and Ahn 2013).

#### 2.4.3 Combination of microfiltration, sedimentation and wetting contrast

Park et al. (2016) have combined microfiltration, sedimentation and wetting contrast to overcome the disadvantages associated with each of these strategies in accomplishing plasma separation. The device consists of PDMS and glass layers for optical transparency. The PDMS layer has inlet, main channel, a large chamber with a dense microarray and an outlet, as shown in Fig. 5. The main channel is of cross section  $300 \mu\text{m} \times 6 \mu\text{m}$  to prevent the entry of WBCs. The narrowly spaced micropillar array is used for partial separation and delay. From the main channel, only RBCs enter the next section where the dense micropillar array of



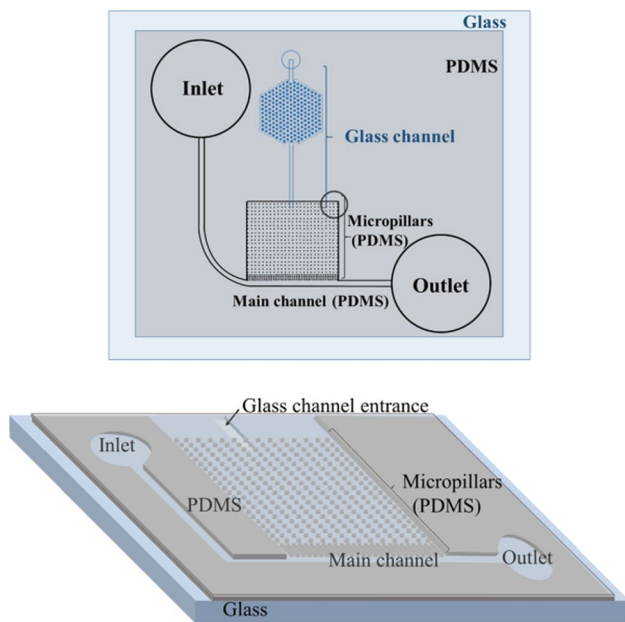


**Fig. 5** Image showing the top and side views of the microfluidic device with glass substrate for capillary flow and large chamber with micropillar array for plasma separation (Park et al. 2016)

spacing  $2.0\ \mu\text{m}$ , placed near the main channels and extending into the main channel filters some of the RBCs. However, the RBCs are elastic and deformable and can navigate through the micropillars. The sudden large expanded cross-sectional area of the chamber delays the flow facilitating the sedimentation of blood cells that have escaped through the filter due to their deformability, as they are denser than plasma ( $\rho_{\text{rbc}} = 1125\ \text{kg/m}^3$ ,  $\rho_{\text{plasma}} = 1025\ \text{kg/m}^3$ ). Contact angle of water and blood varies on ethanol-treated PDMS (water— $97.1^\circ$ , blood— $58.4^\circ$ ) and glass (water— $32.3^\circ$ , blood— $18.4^\circ$ ). Therefore, in the device channel, surface wettability of blood cells and plasma varies at the three PDMS channel walls (ethanol-treated) and glass bottom which leads to varying capillary velocities as evident from Eq. (1). This wettability difference also plays a role in the plasma separation as there is a significant delay in the movement of blood cells while the plasma moves forward. Thus, the sedimentation of RBCs and variation in surface wettability together leads to the advancement of plasma leaving the cells behind. A glass channel of  $2.0\ \mu\text{m}$  depth extends from the chamber area and opens into a large detection area. The hydrophilic nature of the glass channel extracts the plasma from the chamber by capillary effect. Using  $15\ \mu\text{l}$  of whole blood with this device, only  $16\ \text{nl}$  of plasma was obtained but the purification efficiency was found to be approximately 100%.

The features prompting capillarity, the separation principle and performance of the devices presented above are summarized in Table 1. Among the different methods, the

simplest method to bring about capillary-driven flow is to use substrates such as glass, silicon or to treat the biocompatible polymers (e.g. PDMS, PMMA) with oxygen plasma. Oxygen plasma-exposed methyl silsesquioxane (spin-on-glass film, SOG) is reported to provide a biocompatible surface inside micro-chambers of silicon and glass owing to its hydrophobic recovery (Bhattacharya et al. 2010). Reusability of microchannels for DNA amplification by preventing non-specific binding of DNA molecule in the hydrophobic interiors has been reported by Bhattacharya et al. (2007) where silicon is coated with SOG and the PDMS and SOG-coated substrates have been exposed to oxygen plasma at 20 W reactive ion etching (RIE) power, 900 mtorr chamber pressure, 182 sccm oxygen flow rate and 35 s time of exposure. Following an amplification process, a wash cycle comprising a 20-min wash with elution buffer followed by RNase-free water for 10 min was found to render the channel reusable. Similar procedure can be investigated for the reusability of the above-mentioned devices. Further, it is observed that devices employing sedimentation phenomenon provide maximum plasma recovery but the plasma separation using this technique is time consuming (10–20 min). On the other hand, devices employing filtration phenomenon take less time (2–5 min) for the plasma separation but offer the least volume of plasma in spite of the complex geometries used. More importantly, these devices are fully self-powered and self-driven, simple, cost-effective and show good potential in the development of lab-on-chip diagnostics for resource poor settings.

### 3 Capillary-driven blood plasma separation: active techniques

In this section, we enumerate capillary-based blood plasma separation devices reported in the literature which use active energy, i.e. dielectrophoresis forces, to bring about the plasma separation from the sample blood. The driving force for the capillary movement is produced by the surface property of the substrate material and appropriate design of the microchannel geometry. Use of external force in such devices gives rise to higher plasma recovery. The mechanical, electrical and magnetic properties of the blood cells and plasma are given in Table 2.

When blood cells, which are polarizable, are exposed to a non-uniform electric field, the cells experience an induced motion which is termed as dielectrophoresis (Morgan and Green 2003). Electric charges induced at the cell–medium interface in an inhomogeneous electric field create dipoles which get aligned parallel to the applied electric field. The unequal Coulombic forces on the dipoles results in a net force on the cells. Depending on their relative polarizability with reference to the medium, the cells get attracted or

**Table 1** Summary of passive techniques used for capillary-driven blood plasma separation reported in literature

References	Capillary actuation	Separation principle	Device performance
Dimov et al. (2011)	The PDMS device is activated by degassing in vacuum (15 min). Blood sample is introduced within 2 min	Sedimentation in filter trenches	Sample: whole blood Vol of sample: 5 $\mu$ l Time: 10 min Purification efficiency: 99–100% Biological validation: detection of spiked biotin
Son et al. (2014)	Degassing in vacuum chamber	Sedimentation and filtration in a vertical up-flow chamber with a membrane filter (0.4 $\mu$ m pore size) on top	Sample: whole blood Vol of plasma: 2.4 $\mu$ l Time: 20 min Plasma recovery: 20% Biological validation for absence of haemolysis and recovery of protein and cDNA
Kuroda et al. (2014)	Degassing in a vacuum desiccator (20 min). Blood sample introduced within 2 min	Sedimentation of blood cells and ascension of plasma in a cylindrical channel	Sample: blood (10% haematocrit) Time: 20 min
Kim et al. (2010)	PDMS mixed with non-ionic surfactant (Silwet L-77) and SU8 microstructures	Planar cross-flow filtration using shallow channels	Sample: whole blood Vol of sample: 10 $\mu$ l Vol of plasma: 20 nl Plasma recovery: 0.4% Purification efficiency: 100%
Madadi et al. (2015)	PDMS mixed with non-ionic surfactant (Silwet L-77) and etched glass	Filtration with the help of constriction channel and diamond micropost arrays	Sample: whole blood Vol of sample: 5 $\mu$ l Vol of plasma: 0.1 $\mu$ l Time: 5 min Plasma recovery: 4% Purification efficiency: 98%
Khumpuang et al. (2007)	Silicon and glass substrates. Hydrophilicity was increased by oxidation of Si	Filtration using tapering microchannels	Biological validation: On-chip detection of thyroid-stimulating hormone (TSH)
Wu et al. (2012)	Glass substrate and oxygen plasma-treated PDMS	Dead-end filtration using weir-type PDMS microfilter	Sample: special treated human blood (LC-TROL 20 N, R&D System Inc., USA) Vol of sample: 20 $\mu$ l Vol of plasma: $\ll$ 1 $\mu$ l Time: 2 min
Sakamoto et al. (2012)	Oxygen irradiation of PMMA microchannels followed by poly-L-Lysine coating	Filtration using array channels (2 $\mu$ m deep)	Sample: blood (Haematocrit $\leq$ 20%) Biological validation: Detection of electro-active species (ascorbic acid, uric acid, acetaminophen, etc.) with on-chip iridium tin oxide (ITO) electrodes
Lee and Ahn (2013)	Silica nanobead multilayers spray coated on COC substrate	Flow barrier created by hydrophobic patch (uncoated COC polymer)	Sample: whole blood Vol of sample: 20 $\mu$ l Vol of plasma: 150 nl Time: 3 min Plasma recovery: 1.5% Purification efficiency: 99%
			Sample: whole blood Vol of blood: 3 $\mu$ l Vol of plasma: 102 nl Time: 10 min Plasma recovery: 6.8%

Table 1 continued

References	Capillary actuation	Separation principle	Device performance
Maria et al. (2016)	Oxygen plasma-treated PDMS	Flow barrier created by hydrophobic region (unexposed PDMS)	Sample: whole blood Vol of blood: 4 µl Vol of plasma: 450 nl Time: 15 min Plasma recovery: 22.5% Purification efficiency: comparable with centrifugation Biological validation—on-chip glucose test
Maria et al. (2017)	Oxygen plasma-treated PDMS	Sedimentation in an up-flow well and flow barrier (less hydrophilic region in the well)	Sample: whole blood Vol of blood: <10 µl Vol of plasma: 2 µl Time: 15 min Plasma recovery: 40% Purification efficiency: 99% Biological validation—on-chip glucose test
Park et al. (2016)	Glass substrate	Filtration of WBCs by main channel and RBCs by dense micropillar array, sedimentation in large chamber, wetting contrast of blood and plasma with PDMS and glass.	Sample: Whole blood Vol of blood: 15 µl Vol of plasma: 16 nl Plasma recovery: 0.2% Purification efficiency: 100%

repelled from the regions of maximum field strength. The dielectrophoresis force can be expressed as,

$$F_{DEP} = 2\pi \epsilon_m r^3 \text{Re}(f_{CM}) \Delta E_{rms}^2 \tag{16}$$

where  $\epsilon_m$  is the permittivity of the medium,  $r$  is the radius of the cell,  $\text{Re}(f_{CM})$  is the real part of the Clausius–Mosotti factor and  $E_{rms}$  is the root mean square value of the electric field. The parameter  $\text{Re}(f_{CM})$  decides whether the induced force on the cell is repulsive or attractive and  $f_{CM}$  is given as,

$$f_{CM} = \frac{\epsilon_{cell}^* - \epsilon_m^*}{\epsilon_{cell}^* + 2\epsilon_m^*} \tag{17}$$

where  $\epsilon_{cell}^*$  and  $\epsilon_m^*$  are the complex permittivities of the cell and the medium, respectively,  $\epsilon^* = \epsilon - j\frac{\sigma}{\omega}$  where  $j = \sqrt{-1}$ ,  $\epsilon$  is the real permittivity,  $\sigma$  is the electric conductivity and  $\omega$  is the angular frequency of the AC electric field. When the permittivity of the particle is more than that of the medium,  $\text{Re}(f_{CM})$  is positive and the DEP force is attractive, which is known as positive DEP (pDEP). On the other hand, when the permittivity of the particle is less than that of the medium,  $\text{Re}(f_{CM})$  is negative and the force is repulsive, which is known as negative DEP (nDEP). The relative permittivity and electric conductivity of blood cell are 63 and 1.0 µS/m, respectively (Jung and Kwak 2007). RBCs present nDEP when conductivity of blood plasma is more than 0.3 S/m (Szydzik et al. 2015).  $\text{Re}(f_{CM})$  of RBCs is negative as it is less polarizable than the medium; therefore, RBCs exhibit nDEP and get attracted towards the region of lower electric field (Mohammadi et al. 2015).

Nakashima et al. (2010) investigated the use of dielectrophoresis force to separate plasma from electro-capillary-driven blood sample in a microchannel device, as shown in Fig. 6a. The microchannel design has a main channel to draw in blood into the device due to capillary flow and an array of side channels of 5 µm width, 1.0 mm length and 2 µm depth for the filtration of plasma due to cross-flow filtration. However, due to much smaller width of the side channels, the blood cells tend to clog the entrance of the side channels and impede the flow of plasma into these channels. These cells blocking the entrance of the side channels are removed by applying an AC voltage of 10 V and 1.0 MHz between a pair of dissimilar electrodes (pinned and structured electrodes) across the main channel. The inhomogeneous electric field generated between the two electrodes imparts a negative dielectrophoretic force on the blood cells, which moves them towards the lower electric field region. As a result, the blood cells clogging the entrances of the side channels are repelled from the pinned-electrode and get trapped at the structured electrode thus improving the plasma filtration. By using 5.0 µl of blood sample (of dilution 1:9), 300 nl of plasma was extracted and the purification efficiency was calculated to be 97%.

**Table 2** Properties of blood cells and plasma

Properties	Blood cells	Plasma
Mechanical properties (Maria et al. 2016; Furlani 2007; Kim et al. 2012)	Percentage of RBCs by volume—45% Percentage of WBCs by volume—0.7% Size of RBC— $8 \times 2 \mu\text{m}$ Size of WBC—10–15 $\mu\text{m}$ Viscosity of blood, $\mu_{\text{blood}} = 0.00287 \text{ Pa}\cdot\text{s}$ Volume of RBC, $V_{\text{rbc}} = 88.4 \mu\text{m}^3$ Volume of WBC, $V_{\text{wbc}} = 524 \mu\text{m}^3$ Density of RBC, $\rho_{\text{rbc}} = 1100 \text{ kg/m}^3$ Density of WBC, $\rho_{\text{wbc}} = 1070 \text{ kg/m}^3$ Young's modulus of RBC, $E = 4.4 \pm 0.6 \text{ kPa}$ Bending elastic modulus of RBC, $B = 43.5 K_{\text{B}}T$ Area expansion modulus of RBC, $K = 450 \text{ mN/m}$ Shear modulus of RBC, $\mu = 9 \pm 1.7 \mu\text{N/m}$	Percentage by volume—54.3% Viscosity, $\mu = 0.0012 \text{ Pa}\cdot\text{s}$ Density, $\rho = 1000 \text{ kg/m}^3$
Electrical properties (Nakashima et al. 2010; Szydzik et al. 2015)	Relative permittivity, $\epsilon^* = 63$ Electrical conductivity, $\sigma = 1 \mu\text{S/m}$	Relative permittivity, diluted plasma $\epsilon^* = 80$ Electrical conductivity, diluted plasma $\sigma = 55 \text{ mS/m}$ Electrical conductivity, undiluted plasma $\sigma = 1.2 \text{ S/m}$
Magnetic properties (Furlani 2007)	$\chi_{\text{rbc,oxy}} \sim -9.22 \times 10^{-6}$ (Diamagnetic) $\chi_{\text{rbc,deoxy}} \sim -3.9 \times 10^{-6}$ (Paramagnetic) $\chi_{\text{wbc}} \sim -9.9 \times 10^{-6}$ (Diamagnetic)	$\chi_{\text{plasma}} \sim -7.7 \times 10^{-6}$

A similar concept was employed by Szydzik et al. (2015). Here, in addition to the above, post-structures were used to facilitate cross-flow filtration of plasma from undiluted blood, as shown in Fig. 6b. Plasma is extracted through 1.2- $\mu\text{m}$ -deep side channels supported by a repetitive post-structure which acts as a cross-flow filter. The 1.2- $\mu\text{m}$ -deep channels open into a 25- $\mu\text{m}$  plasma extraction capillary pump through a wedge-shaped capillary transition enhancer structures. Dielectrophoresis forces (8 V peak-to-peak, 1.0 MHz AC signal) were used to actively unblock the filter post-structures to enhance the extraction of plasma. Considering that the conductivity of undiluted plasma is 1.2 S/m, though nDEP is strongest at frequencies <100 kHz, here 1.0 MHz is applied in order to minimize thermal stress on cells. The device offers higher plasma recovery (165 nl from 15  $\mu\text{l}$  whole blood) compared to other similar works, but the volume of plasma is still considerably low. Also, the microelectrodes and very shallow plasma extraction channels involve fabrication complexity.

The blood plasma separation device reported by Mohammadi et al. (2015) consists of a straight PDMS channel with dead-end branches on either side at regular intervals bonded to a cover glass as shown in Fig. 6c. It utilizes DC insulator-based electrophoresis for the separation of blood cells. Inhomogeneous electric field is generated by dielectric and low permittivity posts in the

channel which modifies the distribution of the electric field. The use of DC field also eliminates the requirement of external driving force since it can produce electro-osmotic force (EOF). Two electrodes are located at the inlet and outlet. When the blood enters through the inlet of the device by capillary effect, before the electric field (50 V) is applied, the RBCs are captured in the dead-end branches due to hydrodynamic effects. As soon as the electric field is applied, the RBCs get trapped in the first three constrictions from the inlet due to dielectrophoretic phenomenon, thus preventing the entry of more RBCs into the straight channel. Meanwhile, the electro-osmotic flow generated in the centre of the channel as a result of the electric field sweeps the remaining RBCs in the channel creating an RBC-free zone of plasma in the middle of the channel. An electrical double layer is formed on the glass when the DC is applied and the ions are attracted towards the negative electrode thus producing an electro-osmotic flow. For the trapping of cells, the DEP velocity must overcome linear electrokinetic velocity dominated by EOF. Therefore, the condition for the trapping of RBC is

$$\frac{C\mu_{\text{DEP}}\nabla(\vec{E} \cdot \vec{E}) \cdot \vec{E}}{\mu_{\text{EK}}\vec{E} \cdot \vec{E}} > 1 \quad (18)$$



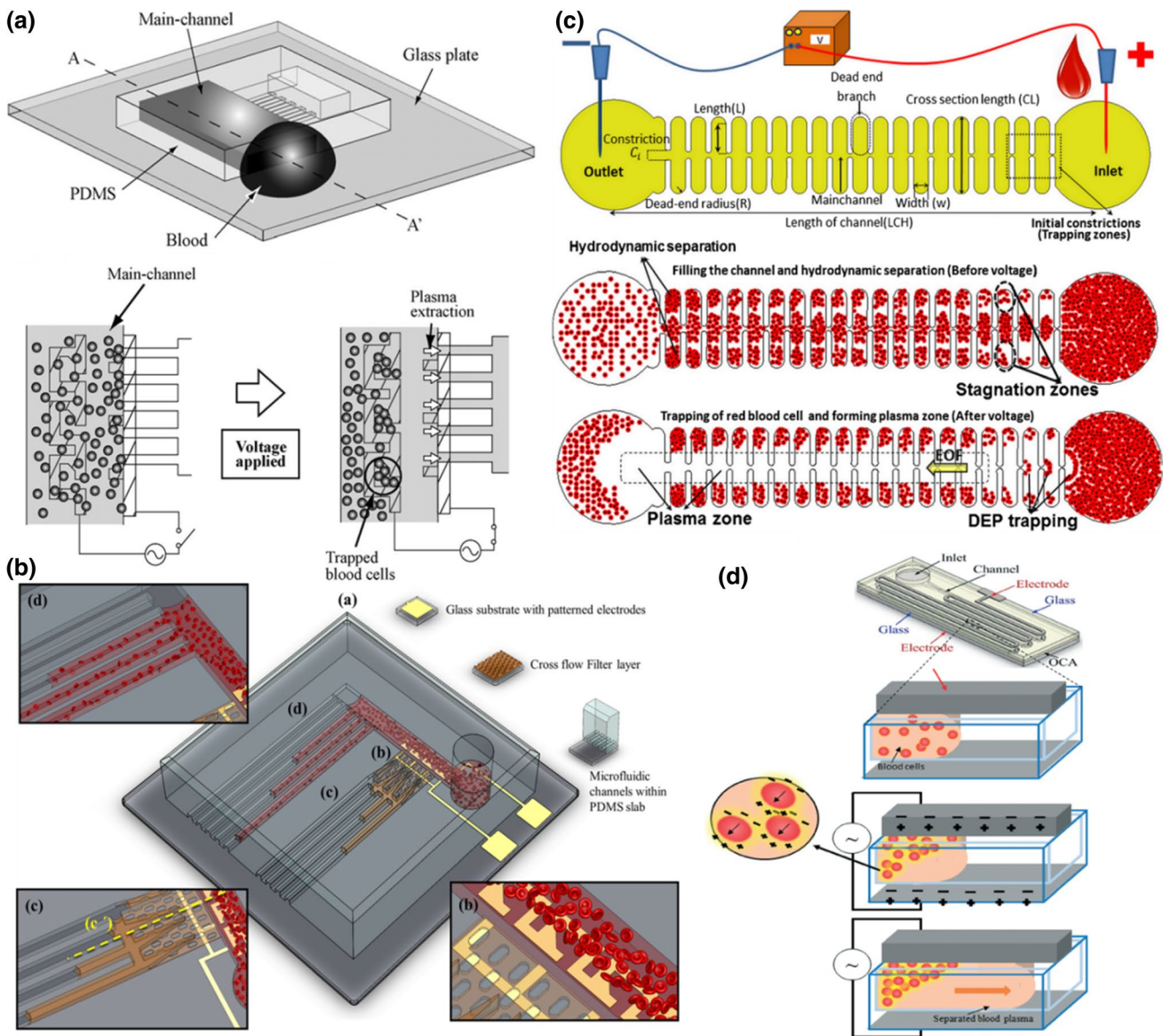


**Fig. 6** Images showing microfluidic devices that exploit dielectrophoresis forces for plasma extraction with glass substrates and device geometry for capillary actuation (Nakashima et al. 2010; Szydzik et al. 2015; Mohammadi et al. 2015; Chen et al. 2014)

where  $C$  is the correction factor,  $\mu_{DEP}$  is the dielectrophoretic mobility,  $\vec{E}$  is the electric field and  $\mu_{EK}$  is the electrokinetic velocity dominated by electro-osmotic mobility  $\mu_{eo}$ .

$$\mu_{DEP} = \frac{r^2 \epsilon_m f_{CM}}{3\eta} \quad (19)$$

where  $r$  is the particle radius,  $\epsilon_m$  is the medium permittivity,  $f_{CM}$  is the Clausius–Mossotti factor and  $\eta$  is the viscosity of the medium. Electro-osmotic mobility  $\mu_{eo}$  is given by

$$\mu_{eo} = \frac{\epsilon_m \zeta_w}{\eta} \quad (20)$$

where  $\zeta_w$  is the zeta potential of the microchannel. A plasma volume of 0.1  $\mu\text{l}$  was obtained from 2.0  $\mu\text{l}$  of blood (dilution

1:1) in 7 min with 99% purification efficiency. This work reported a combination of hydrodynamic separation and DC insulator-based dielectrophoretic forces for plasma separation for the first time and exhibits higher plasma purity, lower processing time and use of lower voltage. However, it does not report collection of the separated plasma from the device. The authors claim that the glass cover that closes the channel could be previously coated with purified proteins or extracellular matrices produced by cells in culture for interaction with plasma analytes for detection. The interacting platelets can also be quantified by means of digital image analysis in haemostasis studies. So, it requires continuous application of electric field throughout in order to keep the RBCs away from the plasma zone. Also, care should

be taken such that the coating is carefully patterned to the RBC-free zone.

In a different context but with similar concept, Ghubade et al. (2009) has reported a dielectrophoresis-activated cell sorting (DACS) which concentrates fluorescent beads by dielectrophoresis and locally concentrates them in a microchannel. An alternating voltage of 1 Vp-p for a range of different frequencies across finely placed interdigitated microelectrodes help in the capture of the flowing beads. They have demonstrated rapid quantification of beads from the different rates of growth of the fluorescent signals. The authors claim that the device can be used for detection of fluorescent-marked pathogens in a sample.

Active separation can cause considerable damage due to the large magnitude of forces acting on the cells (Maria et al. 2015). The high voltage used can rupture RBCs and release haemoglobin into the plasma resulting in reduced quality of plasma. Chen et al. (2014) reported a portable, disposable, capillary-driven microfluidic device for plasma separation which operates at lower AC voltage (1.0 Vp-p) and with contactless dielectrophoresis. These can overcome the damage to RBCs and release of haemoglobin caused by high voltage. The absence of contact between electrodes and blood sample helps in preventing bubble formation, heat production and contamination of electrodes. The device is fabricated with two glass slides forming the top and bottom walls of the channels and optically clear adhesive forms the side walls. The top electrode is sputter coated only above the channel area, and bottom electrode is sputter coated wholly below the bottom slide. The electrodes are capacitively coupled to the microfluidic channel. The blood sample is driven into the device by capillary force based on contact angle, geometry of the device and the surface tension. An inhomogeneous high-frequency electric field is applied to the electrodes induce an electrostatic force between the cells in the channel. A velocity difference is imparted between the cells and the plasma as a result of dielectrophoretic effect on the polarized, aggregated cells and the capillary force. Thus, the plasma separates from the blood cells as observed in Fig. 6d. The device demonstrated a purification efficiency of 89.4% and plasma recovery of 69.8% with minimal haemolysis from a blood volume of 150  $\mu\text{l}$ .

Table 3 presents a summary of the capillarity feature, separation principle and device performance of the above-mentioned works. Maximum plasma recovery (69.8%) has been reported by Chen et al. (2014) with low-voltage contactless dielectrophoresis, but the purification efficiency is considerably reduced. The listed devices have used glass substrates to induce capillary movement of sample in the device. Compared to some of the passive separation devices, higher plasma volume was obtained with the employment of dielectrophoresis forces in these devices.

#### 4 Paper microfluidics for blood plasma separation

Significant research effort has been put in the development of microfluidic paper-based analytical devices ( $\mu\text{PADs}$ ) from patterned paper, based on colorimetric assays, for point-of-care diagnosis. Diagnostic tests based on lateral flow immunoassay or dipstick tests, chromatography and electrophoresis use paper as the supporting medium (Songjaroen et al. 2012). The flow of fluid through the paper-matrix composed of randomly distributed cellulose fibres occurs due to the capillary imbibition through the inter-fibre passages (Kar et al. 2015). When paper is immersed in liquid, a pressure gradient is created at the dry and wet side of the paper. The pressure difference drives the capillary flow into the  $\mu\text{PAD}$  (Kumar et al. 2016). The pressure difference over a wetted region of paper strip of length  $l$  is given as,

$$\Delta P = -\frac{2\gamma \cos \theta}{r_a} \quad (21)$$

where  $\gamma$  is the interfacial surface tension,  $\theta$  is the contact angle of the liquid with the paper and  $r_a$  is the average pore radius. Therefore, the pressure decreases with distance as the fluid moves up the strip. The position of liquid front at given time  $t$  is given by,

$$l(t) = 2\sqrt{\frac{k_i \gamma \cos \theta}{r_a}} \sqrt{t} \quad (22)$$

where  $k_i = k/\phi$ , interstitial permeability of the paper strip,  $\phi$  is the porosity of the medium.

The  $\mu\text{PAD}$  technology offers substantial advantages such as reduced time, resources, and infrastructure to produce traditional diagnostic devices. Being compact, inexpensive and simple to use makes it well suited for implementation in the developing world and other resource-limited settings (Yang et al. 2012). To avoid sample preparation (plasma separation) by centrifugation or specifically designed devices with fine features before introducing plasma sample into the  $\mu\text{PAD}$ , several studies have been performed on the plasma separation on paper.

The first  $\mu\text{PAD}$  for plasma separation was reported by Yang et al. (2012) which used the phenomenon of RBC agglutination. The effective size of RBCs increases as a result of formation of large multi-cellular aggregates which can be filtered using a filter with pore size significantly larger than 2.5  $\mu\text{m}$ . Also, purified plasma can be obtained at a much higher volumetric flow rate. In this device, Anti-A,B, the monoclonal antibodies which selectively bind to antigen A and antigen B present on the surface of human RBCs, were used to induce RBC agglutination. The pattern of the  $\mu\text{PAD}$  was made by drawing lines using solid ink on

**Table 3** Summary of active techniques used for capillary-driven blood plasma separation reported in the literature

References	Capillary actuation	Separation principle	Device performance
Nakashima et al. (2010)	Glass substrate	Filtration through side channels. Dielectrophoresis forces unblock channel entrances	<p>Device size:                      Main channel—500 <math>\mu\text{m}</math> (w) <math>\times</math> 20 mm (l) <math>\times</math> 100 <math>\mu\text{m}</math> (d)                      Side channels—5 <math>\mu\text{m}</math> (w) <math>\times</math> 1 mm (l) <math>\times</math> 2 <math>\mu\text{m}</math> (d)                      Plasma reservoir—3 mm (w) <math>\times</math> 3 mm (l) <math>\times</math> 100 <math>\mu\text{m}</math> (d)                      Width of electrode—60 <math>\mu\text{m}</math>                      Interdistance—30 <math>\mu\text{m}</math>                      Electric field: 10 V and 1.0 MHz (AC)                      Sample: blood (dilution 1:9)                      Vol of sample: 5 <math>\mu\text{l}</math>                      Vol of plasma: 300 nl                      Plasma recovery: 12%                      Purification efficiency: 97%</p>
Szydzik et al. (2015)	An array of PDMS channels (parallel 100 $\mu\text{m}$ wide, 25 $\mu\text{m}$ deep) on a glass substrate forms the capillary pump	Filter post-structures. Dielectrophoresis forces unblock filter structures.	<p>Device size:                      Primary channel—500 <math>\mu\text{m}</math> (w) <math>\times</math> 25 <math>\mu\text{m}</math> (d)                      Cross-flow filter—1.2-<math>\mu\text{m}</math> capillary pump                      Array of channel—100 <math>\mu\text{m}</math> (w) <math>\times</math> 25 <math>\mu\text{m}</math>                      Electric field: 8 V, 1 MHz (AC)                      Sample: whole blood                      Vol of sample: 15 <math>\mu\text{l}</math>                      Vol of plasma: 165 nl                      Time: 15 min                      Plasma recovery: 2.2%</p>
Mohammadi et al. (2015)	Cover glass substrate	Dielectrophoretic phenomenon traps RBCs in first three constrictions. Electro-osmotic force sweeps remaining RBCs forming RBC-free plasma zone	<p>Device size:                      Centre channel—1 cm (l) <math>\times</math> 50 <math>\mu\text{m}</math> (d)                      Dead branches—200 <math>\mu\text{m}</math> (l) <math>\times</math> 50 <math>\mu\text{m}</math> (d)                      Electric field: 50 V (DC)                      Sample: blood (dilution 1:1)                      Vol of sample: 2 <math>\mu\text{l}</math>                      Vol of plasma: 0.1 <math>\mu\text{l}</math> plasma                      Time: 7 min                      Plasma recovery: 10%                      Purification efficiency: 99%</p>
Chen et al. (2014)	Glass substrates on top and bottom	Low-voltage contactless dielectrophoresis imparts velocity difference between cells and plasma	<p>Device size: 7.5 cm (l) <math>\times</math> 3.5 cm (w)                      Microchannels—800 <math>\mu\text{m}</math> (w) <math>\times</math> 175 <math>\mu\text{m}</math> (d)                      Electric field: 1 V, 1 MHz (AC)                      Sample: whole blood                      Vol of sample: 150 <math>\mu\text{l}</math>                      Plasma recovery: 69.8%                      Purification efficiency: 89.4%                      Biological validation of minimal haemolysis</p>

a chromatographic paper and heating the printed chromatographic paper on a hot plate (150 °C, 3 min). The centre of the  $\mu$ PADs was functionalized by spotting the anti-A,B antibody solution. Thus, when a drop of whole blood was placed directly onto the plasma separation zone of the device, the RBCs agglutinated and remained in the central zone, while the separated plasma wicked through the paper substrate as shown in Fig. 7a. Though simple and novel, the addition of antibodies increases the cost of the device significantly.

Songjaroen et al. (2012) used LF1 blood separation membrane (polyvinyl alcohol-bound glass fibre filters) in combination with a patterned filter paper for the separation as shown in Fig. 7b. The device was fabricated by wax dipping method. Here, patterned iron mould was first placed over an arrangement where Whatman No.1 paper and blood separation membrane were overlapped approximately 1.0 mm on a glass slide, and held in place by a permanent magnet behind the glass slide. This set-up was then dipped into melted beeswax for 1.0 s and cooled. The paper was peeled off the glass slide and used for plasma separation. Thus, the blood separation membrane forms bottom part of  $\mu$ PAD which traps the blood cells in the sample blood. The separated plasma flows through the Whatman No. 1 membrane which forms the top part of the  $\mu$ PAD. Plasma was effectively separated from human whole blood of 24–55% haematocrit without dilution within 2 min when blood volumes of between 15 and 22  $\mu$ l were added to the device. The device is simple, rapid, low-cost, portable, disposable and single-step diagnostic platform for real-world sample. However, the efficiency of the device is highly dependent on the volume of blood added to the device. If large volume is added, blood cells will overflow from separation zone to the detection zone, resulting in contamination of the plasma, whereas too little sample may lead to inadequate plasma yield in the detection zone.

Similar work by Noiphung et al. (2013) reports a  $\mu$ PAD device, made of two VF1 plasma separation membranes (binder-free glass fibre filter) and a Whatman filter paper fabricated by wax dipping technique as shown in Fig. 7c. The final device was of dumbbell shape, composed of two blood separation zones on either sides and a middle detection zone. Generally, device with a single sample separation zone, as in Songjaroen et al. (2012), can lead to uneven plasma flow over the detection zone, hence generating irreproducible electrochemical signals. The dumbbell shape generates homogeneous flow of separated plasma to the electrode at the detection zone of the ePAD for much better reproducibility of electrochemical signals. The variation of time of separation of plasma from samples of different haematocrit was also reduced. Blood sample of 24–60% haematocrit without dilution was added to the device, and the plasma was completely separated within 4.0 min.

Kar et al. (2015) demonstrated simple H-channels, a two-dimensional paper-based network as shown in Fig. 7d, devoid of elaborate and complex instrumentation, and the usage of expensive consumables. It works on the principle of capillarity-driven diffusion of analyte molecules. The device, fabricated using origami-based protocol, has two reservoirs, each for blood sample and PBS, a straight common channel followed by two outlets. The blood and PBS placed at respective reservoirs are pulled into the cellulose fibres and flow simultaneously in the straight channel where the lighter molecules (having low molecular weight) suspended within the blood stream diffuse into the adjacent PBS stream. Diffusion of the lighter molecules increases with distance and gets collected at reservoir B1. The authors have drawn a parallel between this diffusion of analytes into the buffer stream and plasma separation. They claim the separation efficiency to be  $75.4 \pm 9.1\%$  for a device having a width of 5 mm and a length of 3 cm, from comparison of greyscale intensities at the outlets. Though this device does not require state-of-the-art instrumentations, trained personnel or sophisticated laboratory environment, the extent and quality of plasma separation is not reported and uncertain.

The paper fluidic devices are the simplest, easy to operate, flexible, portable and inexpensive blood separation platforms (Liana et al. 2012). The paper fluidic devices for plasma separation reported above are summarized in Table 4. Though plasma separation has been observed in these devices, the plasma quality, i.e. volume and purity, remains unknown. Due to the small pore sizes of fibres, the volume of plasma in the detection zone is very low which could impact the detection of analytes at low concentration. A detailed description of the limitations of paper fluidic devices is presented by Li et al. (2012).

## 5 On-chip detection in capillary-based plasma separation devices

In some of the above-mentioned works, in addition to the blood plasma separation, on-chip detection of analytes present in the plasma has been demonstrated. Following the separation, plasma is made to flow into a channel where the plasma analytes are detected by electrochemical, fluorescence or colorimetric assays. Noiphung et al. (2013) demonstrated detection of glucose level in blood samples by electrochemical method. Here, 5.0  $\mu$ l of glucose oxidase ( $645 \text{ U ml}^{-1}$ ) was pre-immobilized at the detection zone in a  $\mu$ PAD. A Prussian Blue screen-printed electrode was placed under this detection zone. Prussian Blue was chosen as the mediator in this work because of its selective catalytic reduction properties for  $\text{H}_2\text{O}_2$ . When whole blood sample was added to both sides of the blood separation device, the plasma separated by the



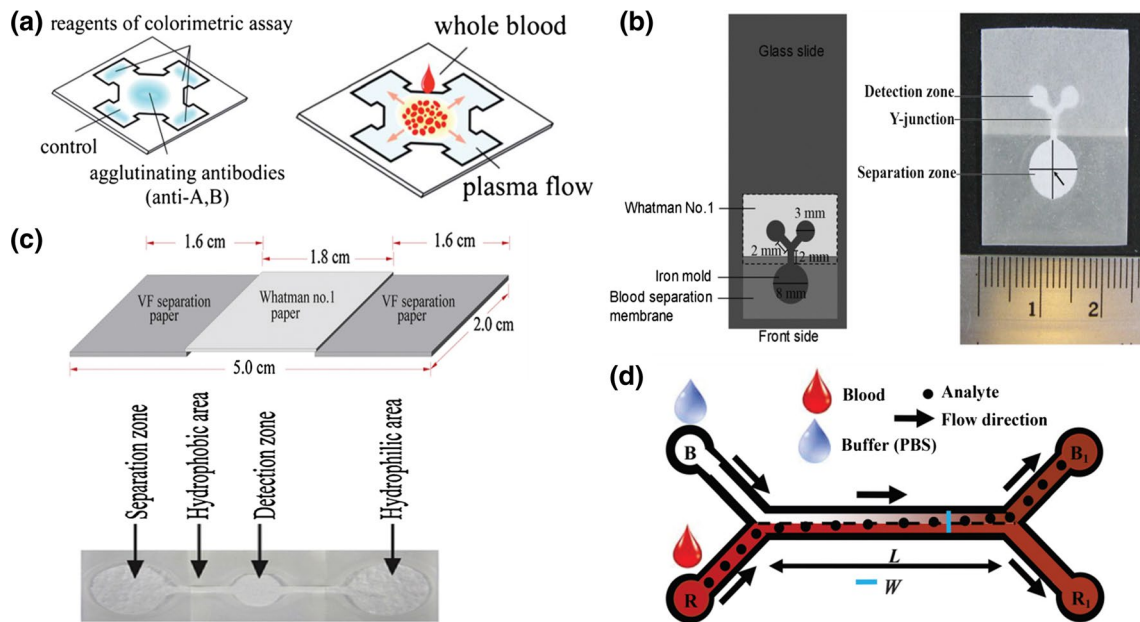


**Fig. 7** Paper microfluidic devices for blood plasma separation fabricated with **a** chromatographic paper and Anti-A,B antibodies (Yang et al. 2012), **b**, **c** filter paper and blood separation membrane (Song-

jaroen et al. 2012; Noiphung et al. 2013) and **d** filter paper with H-channels for blood and PBS buffer (Kar et al. 2015)

membrane penetrated into Whatman filter paper and flowed into the detection zone where it reacted with the glucose oxidase enzyme. The reaction product  $H_2O_2$  (from glucose and oxygen) passes through the filter paper to the surface of the Prussian Blue-modified electrode and was thus detected by measuring the current at a fixed time at a reduction potential of  $-0.10\text{ V}$  (vs  $Ag/AgCl$ ) which gives a measure of the glucose levels. Since  $H_2O_2$  is an enzymatic reaction product of several other biochemical markers, this device (with appropriate enzyme coated at detection zone) can be used for quantitative analytical determinations of various analytes including uric acid, lactate and cholesterol.

Another device with integrated blood plasma separation and electrochemical detection was reported by Wu et al. (2012). Here, the device had an ITO (indium tin oxide)—electrode fabricated onto one of the substrates. The electrochemical properties of the separated plasma were measured by this on-chip electrode using a potentiostat. Ascorbic acid, uric acid and acetaminophen are three most well-known oxidizable species in animal tissues and fluids. The cyclic voltammograms measured for the blood samples in the device showed the detection of these electroactive species which are capable of being initially oxidized at  $+0.4\text{ V}$  versus the ITO reference electrode. Therefore, the authors assert that the microfilter device is feasible for use in a micro-total analysis system chip for blood analysis.

In the SIMBA device reported by Dimov et al. (2011), in the channel where the separated plasma flows, termed as bio-recognition site, the top glass slide was patterned

with  $15\text{-}\mu\text{m}$ -wide lines of avidin by microcontact printing, perpendicular to the flow direction. The blood sample was spiked with fluorescent labelled biotin, and the detection was performed by streptavidin–biotin assay. The device was disassembled, and the top slide was analysed in a microarray scanner for the fluorescent readout. Biotin concentration as low as  $1.5\text{ pM}$  was detected with the device within 10 min. As stated by the authors, the suction chamber volume and the binding site surface area need to be modified to compensate for the low sensitivity in the case of clinically relevant biomarkers. This is because, when compared to the streptavidin–biotin used in this study, the biomarkers could have lower antibody–antigen on-rates and higher equilibrium dissociation rates.

Colorimetric assay was demonstrated by Yang et al. (2012) for glucose determination. The fabricated  $\mu\text{PAD}$  device had three rectangular test read out zones. Three of the zones were functionalized with  $1.0\text{ }\mu\text{l}$  of the solution containing the reagents of the colorimetric assay, and the remaining zone was treated with  $1.0\text{ }\mu\text{l}$  PBS solution. A blood droplet ( $7\text{ }\mu\text{l}$ ) was placed at the centre of the  $\mu\text{PAD}$  which is functionalized with anti-A,B antibodies which retains the RBCs by agglutination. The plasma flows into the test read zones where the glucose oxidase catalyses the oxidation of the plasma glucose and produces  $H_2O_2$  which reacts with potassium iodide catalysed by horseradish peroxidase giving brown colour. The intensity of colour change is proportional to the amount of glucose in sample plasma. The PBS-treated test zone was used

**Table 4** Summary of paper fluidic devices used for capillary-driven blood plasma separation reported in literature

References	Capillary actuation	Separation principle	Device performance
Yang et al. (2012)	Solid ink lines on chromatographic paper	Pattern drawn using solid ink printer and heated on a hot plate (150 °C, 3 min). Centre of the mPAD functionalized with antibodies	RBC agglutination by Anti-A,B antibodies
Songjaroen et al. (2012)	Whatman No.1 filter paper and LF1 blood separation membrane overlapped (1 mm)	Wax dipping method	Blood cells are trapped by blood separation membrane. Plasma flows through the filter paper
Noiphung et al. (2013)	Two VF1 blood separation membranes overlapped with Whatman filter papers (1 mm on each side)	Wax dipping method	Blood cells are trapped by blood separation membrane. Plasma flows through the filter paper. Homogenous flow of plasma to detection zone
Kar et al. (2015)	H-channels made on Whatman No. 4 filter paper	Origami protocol	Diffusion of analytes from blood stream into the buffer stream

as control to subtract the background colour of the separated plasma to improve the accuracy of the colorimetric assay. The colour change was quantified using MATLAB, and the glucose levels can be determined from a calibration curve. In this device, the detection was completed within 5 min. On-chip glucose determination by similar methods has also been reported by Kar et al. (2015) where the plasma reservoir B1 is pre-spotted with glucose oxidase, peroxidase and 4-amino anti-pyrene. The greyscale intensities are measured and correlated with the glucose concentration. As the separation efficiency is 75.4% with this device, the measured values of glucose differ by 10% from the actual value.

Songjaroen et al. (2012) also used colorimetric assay in  $\mu$ PAD for plasma protein detection. It is based on the principle in which bromocresol green (BCG) reacts with proteins to give a significant colour change from colourless to deep blue. In this device, 0.5  $\mu$ l of 10 $\times$  BCG working reagent was dropped on both test zones. The plasma separated by the  $\mu$ PAD membrane penetrates into the test zones and reacts with BCG to give the colour change. The intensity of the colour change was measured with Adobe Photoshop CS2 software, and the quantity of plasma proteins can be determined from the calibration curve of known protein values.

Madadi et al. (2015) and Maria et al. (2016, 2017) have used commercially available test strips to demonstrate on-chip detection with their proposed devices. The plasma separated by the device reported by Madadi et al. (2015) is driven into the lateral flow immunochromatographic NADAL TSH (thyroid-stimulating hormone) test strip to detect TSH, the hormone secreted by pituitary gland. The filtration pad and the absorption pad are removed from the commercial test strip, and the gold conjugated pad is tapped onto the plasma collection reservoir. The gold conjugated antibodies capture the plasma antigens and flow to the test line where these nanoparticle complexes form strong bond with the immobilized antibodies embedded in the nitrocellulose membrane. The formation of test line and control lines shows the detection of high levels of TSH in the sample. Maria et al. (Maria et al. 2016, 2017) have used the functionalized surface of the Accu-Chek test strips for detecting glucose in the separated plasma. The strips were located in the region of the channel where the separated plasma flows. Depending on the level of glucose in the plasma, the initially yellow-coloured strip changes to green or blue. The greyscale intensities were measured using ImageJ software and correlated with the actual glucose concentration.

The detection of plasma analytes in the above devices shows that these plasma separation modules are compatible with integrated detection platforms and can be adopted for the development of lab-on-chip diagnostic devices.

## 6 Comparison of capillary-driven plasma separation devices

Although the employment of active energy, i.e. dielectrophoresis, increases separated plasma volume, the increment is not significant. In case of the contactless dielectrophoresis technique reported by Chen et al. (2014), the plasma recovery is 69.8%, which is quite high. However, in this case, the purification efficiency reduces to 89.4%. Also, even with the use of dielectrophoresis, efficient plasma separation requires intricate geometry and shallow channels as in Nakashima et al. (2010) and Szydzik et al. (2015) which require complex fabrication process. On the other hand, with very simple geometry in passive capillary-based plasma separation devices, plasma recovery of 22.5% (Maria et al. 2016) and 40% (Maria et al. 2017) from whole blood sample with 99% purification efficiency has been achieved. The cost and complexity of the passive devices can be further brought down with the use of naturally hydrophilic substrates (Wu et al. 2012; Park et al. 2016; Khumpuang et al. 2007) or hydrophilic PDMS (Kim et al. 2010; Maria et al. 2016, 2017; Madadi et al. 2015). However, such devices could have limitations in terms of the time taken for the plasma separation. Due to the advantages in terms of simplicity and cost and self-powered, self-driven passive plasma separation, such devices are more promising for lab-on-chip diagnostic devices in the field of theranostics. Paper fluidic devices are much simpler and cost-effective compared to microfluidic devices, but the volume of separated plasma flowing through the fibres and reacting with embedded reagents is very low, thus reducing the sensitivity and detection efficiency for low-abundant plasma analytes. While this review presents a guideline, the choice of a suitable plasma separator module would depend on the type of end-user and application.

## 7 Conclusions

This review elucidates the various capillary flow-based techniques for the separation of plasma from sample blood. Both active and passive methods of separation from capillary-driven blood sample have been put forth, discussed and compared. Devices based on passive separation methods, being fully self-powered and cost-effective, are more attractive and simpler than the active devices. However, the plasma recovery in most of the passive devices is lower and the time taken for the plasma separation is higher than that in case of the active devices. In  $\mu$ PAD devices, the sample is self-driven by capillary action through the open spaces between the fibres. The disadvantage with  $\mu$ PADs is that the plasma cannot

be taken out of the device for analysis and the quality of the separated plasma remains unknown. The on-chip detection of analytes performed in some of these devices demonstrates their suitability for lab-on-chip diagnostic devices. Each of the devices reported in the present review would suit different end-users and applications. Evidently, there is no capillary-based plasma separation device, hitherto, that can achieve plasma separation in less time, with high plasma recovery, in a device that is simple, cost-effective and easy to use for accurate diagnosis. The realization of such a device, in future, would require significant research efforts, which can possibly be achieved by combining the advantages of different techniques mentioned in this review. Thus, it is apparent that more research is required in this field as there is an immediate need for an efficient, self-powered, self-driven module for efficient plasma separation for integration with detection platforms.

**Acknowledgements** The authors would like to acknowledge SERB, DST, India (EMR/2014/001151), and IIT Madras (MEE1516843R-FTPASHS) for the financial support.

## References

- Abram E (2015) Screening and Diagnostic Tests. Medscape. <http://emedicine.medscape.com/article/773832-overview>. Accessed 20 Nov 2016
- AdvaMed (2012) Essentials of Diagnostics. DX Insights, pp 1–14
- Aran K, Fok A, Sasso LA, Kamdar N, Guan Y, Sun Q, Undar A, Zahn JD (2011) Microfiltration platform for continuous blood plasma protein extraction from whole blood during cardiac surgery. *Lab Chip* 11:2858–2868
- Bhattacharya S, Datta A, Berg JM, Gangopadhyay S (2005) Studies on surface wettability of poly(dimethyl) siloxane (pdms) and glass under oxygen-plasma treatment and correlation with bond strength. *J Microelectromech Syst* 14(3):590–597
- Bhattacharya S, Gao Y, Korampally V, Othman MT, Grant SA, Kleiboeker SB, Gangopadhyay K, Gangopadhyay S (2007) Optimization of design and fabrication processes for realization of a PDMS-SOG-silicon DNA amplification chip. *J Microelectromech Syst* 16(2):401–410
- Bhattacharya S, Singh RK, Mandal S, Ghosh A, Bok S, Korampally V, Gangopadhyay K, Gangopadhyay S (2010) Plasma modification of polymer surfaces and their utility in building biomedical microdevices. *J Adhes Sci Technol* 24:2707–2739
- Blatter C, Jurischka R, Schoth A, Kerth P, Menz W (2004) Separation of blood cells and plasma in microchannel bend structures. In: *Lab-on-a-Chip: platforms, devices, and applications*, vol 143, pp 143–151
- Chai J, Lu F, Li B, Kwok DY (2004) Wettability interpretation of oxygen plasma modified poly(methyl methacrylate). *Langmuir* 20:10919–10927
- Chen C, Lin P, Chung C (2014) Microfluidic chip for plasma separation from undiluted human whole blood samples using low voltage contactless dielectrophoresis and capillary force. *Lab Chip* 14:1996

- Coulson JM, Richardson JF, Backhurst JR, Harker JH (1991) Chemical engineering volume 2: particle technology and separation processes, 5th edn. Pergamo Press, Oxford
- Crowley TA, Pizziconi V (2005) Isolation of plasma from whole blood using planar microfilters for lab-on-a-chip applications. *Lab Chip* 5:922–929
- Davis JA, Inglis DW, Morton KJ, Lawrence DA, Huang LR, Chou SY, Sturm JC, Austin RH (2006) Deterministic hydrodynamics: taking blood apart. *PNAS* 103:14779–14784
- Dimov IK, Basabe-Desmots L, Garcia-Cordero JL, Ross BM, Ricco AJ, Lee LP (2011) Stand-alone self-powered integrated microfluidic blood analysis system (SIMBAS). *Lab Chip* 11:845–850
- Faivre M, Abkarian M, Bickraj K, Stone HA (2006) Geometrical focusing of cells in a microfluidic device: an approach to separate blood plasma. *Biorheology* 43:147–159
- Furlani EP (2007) Magnetophoretic separation of blood cells at the microscale. *J Phys D Appl Phys* 40:1313–1319
- Ghubade A, Mandal S, Chaudhury R, Singh RK, Bhattacharya S (2009) Dielectrophoresis assisted concentration of microparticles and their rapid quantitation based on optical means. *Biomed Microdevices* 11:987–995
- Hosokawa K, Sato K, Ichikawa N, Maeda M (2004) Power-free poly(dimethylsiloxane) microfluidic devices for gold nanoparticle-based DNA analysis. *Lab Chip* 4(3):181–185
- Hou HW, Bhagat AAS, Lee WC, Huang S, Han J, Lim CT (2011) Microfluidic devices for blood fractionation. *Micro Mach* 2:319–343
- Juncker D (2002) Capillary microfluidic systems for bio/chemistry. Ph.D. Thesis, Université de Neuchâtel, Anorage, p 16
- Jung JY, Kwak HY (2007) Separation of microparticles and biological cells inside an evaporating droplet using dielectrophoresis. *Anal Chem* 79(13):5087–5092
- Kar S, Maitia TK, Chakraborty S (2015) Capillarity-driven blood plasma separation on paper-based devices. *Analyst* 140:6473
- Kersaudy-Kerhoas M, Sollier E (2013) Micro-scale blood plasma separation: from acoustophoresis to egg-beaters. *Lab Chip* 13:3323–3346
- Khumpuang S, Tanaka T, Aita F, Meng Z, Ooe K, Ikeda M, Omori Y, Miyamura K, Yonezawa H, Matsumoto K, Sugiyama S (2007) Blood plasma separation device using capillary phenomenon. In: 14th International conference on solid-state sensors, actuators and microsystems, france, pp 1967–1970
- Kim YC, Kim S, Kim D, Park S, Park J (2010) Plasma extraction in a capillary-driven microfluidic device using surfactant-added poly(dimethylsiloxane). *Sens Actuators B Chem* 145(2):861–868
- Kim Y, Kim K, Park Y (2012) Measurement techniques for red blood cell deformability: recent advances. In: Moschandreu TE (ed) *Blood cell—an overview of studies in hematology*. InTech, Rijeka, pp 167–194
- Kovarik ML, Gach PC, Ornoff DM, Wang Y, Balowski J, Farrag L, Allbritton NL (2012) Micro total analysis systems for cell biology and biochemical assays. *Anal Chem* 84(2):516–540
- Kumar S, Bhushan P, Saha A, Bhattacharya S (2016) Diagnosis of communicable diseases using paper micro-fluidic platforms. In: Cheng C-M, Hsu M-Y, Wu MY-C (eds) *Point-of-care diagnostics—new progresses and perspectives*. IAPC Open Book and Monograph Platform (OBP), Zagreb
- Kuroda C, Ohki Y, Ashiba H, Fujimaki M, Awazu K, Tanaka T, Makishima M (2014) Microfluidic sedimentation system for separation of plasma from whole blood. In: *IEEE sensors 2014 proceedings, Valencia*, pp 1854–1857
- de Laplace PS, Bowditch N (1829) *Méchanique céleste*. Hillard, Gray, Little and Wilkins, Boston
- Lee KK, Ahn CH (2013) A new on-chip whole blood/plasma separator driven by asymmetric capillary forces. *Lab Chip* 13(16):3261–3267
- Li X, Ballerini DR, Shen W (2012) A perspective on paper-based microfluidics: current status and future trends. *Biomicrofluidics* 6(1):011301–011313
- Liana DD, Raguse B, Gooding JJ, Chow E (2012) Recent advances in paper-based sensors. *Sensors* 12:11505–11526
- Madadi H, Casals-Terré J, Mohammadi M (2015) Self-driven filter-based blood plasma separator microfluidic chip for point-of-care testing. *Biofabrication* 7(2):025007
- Manz A, Graber N, Widmer HM (1990) Miniaturized total chemical analysis systems: a novel concept for chemical sensing. *Sens Actuators B* 1(1–6):244–248. doi:10.1016/0925-4005(90)80209-I
- Maria MS, Kumar BS, Chandra TS, Sen AK (2015) Development of a microfluidic device for cell concentration and blood cell-plasma separation. *Biomed Microdevices* 17:115
- Maria MS, Rakesh PE, Chandra TS, Sen AK (2016) Capillary flow based microfluidic device for blood plasma separation and glucose detection. *Biomicrofluidics* 10:054108
- Maria MS, Rakesh PE, Chandra TS, Sen AK (2017) Capillary flow-driven microfluidic device with wettability gradient and sedimentation effects for blood plasma separation. *Sci Rep* 7:43457. doi:10.1038/srep43457
- Mohammadi M, Madadi H, Casals-Terré J, Sellarès J (2015) Hydrodynamic and direct-current insulator-based dielectrophoresis (H-DC-iDEP) microfluidic blood plasma separation. *Anal Bioanal Chem* 407:4733–4744
- Morgan H, Green NG (2003) *AC electrokinetics: colloids and nanoparticles*. Research Studies Press, Baldock
- Mukherjee S, Kang TG, Chen Y, Kim S (2009) Plasma separation from blood: the ‘lab-on-a-chip’ approach. *Crit Rev Biomed Eng* 37(6):517–529
- Nakashima Y, Hata S, Yasuda T (2010) Blood plasma separation and extraction from a minute amount of blood using dielectrophoretic and capillary forces. *Sens Actuators B* 145:561–569
- National Heart, Lung and Blood Institute (2012) *Types of Blood Tests*. US Department of Health and Human Services: National Institutes of Health. <https://www.nhlbi.nih.gov/health/health-topics/topics/bdt/types>. Accessed 18 Nov 2016
- Noiphung J, Songjaroen T, Dungchai W, Henry CS, Chailapakul O, Laiwattanapaisal W (2013) Electrochemical detection of glucose from whole blood using paper-based microfluidic devices. *Anal Chim Acta* 788:39–45
- Park S, Shabani R, Schumacher M, Kim Y, Bae Y, Lee K, Cho HJ (2016) On-chip whole blood plasma separator based on micro-filtration, sedimentation and wetting contrast. *Microsyst Technol* 22:2077–2085
- Pietrangelo A (2015) *Enzyme Markers*. Healthline. <http://www.healthline.com/health/enzyme-markers#Risks4>. Accessed 18 Nov 2016
- Sakamoto H, Hatsuda R, Miyamura K, Sugiyama S (2012) Plasma separation PMMA device driven by capillary force controlling surface wettability. *Micro Nano Lett* 7(1):64–67
- Son JH, Lee SH, Hong S, Park S, Lee J, Dickey AM, Lee LP (2014) Hemolysis-free blood plasma separation Hemolysis-free blood plasma separation. *Lab Chip* 14:2287
- Songjaroen T, Dungchai W, Chailapakul O, Henry CS, Laiwattanapaisal W (2012) Blood separation on microfluidic paper-based analytical devices. *Lab Chip* 12:3392–3398
- Swiss Precision Diagnostics GmbH (1985) *Clearblue Pregnancy Tests*. Clearblue. <http://uk.clearblue.com/>. Accessed 10 Nov 2016
- Szydzik C, Khoshmanesh K, Mitchell A, Karnutsch C (2015) Microfluidic platform for separation and extraction of plasma



- from whole blood using dielectrophoresis. *Biomicrofluidics* 9:064120
- Toner M, Irimia D (2005) Blood-on-a-chip. *Annu Rev Biomed Eng* 7:77–103
- Tripathi S, Kumar YVBV, Prabhakar A, Joshi SS, Agrawal A (2015) Passive blood plasma separation at the microscale: a review of design principles and microdevices. *J Micromech Microeng* 25(8):083001
- Whitesides GM (2006) The origins and the future of microfluidics. *Nature* 442:368–373. doi:[10.1038/nature05058](https://doi.org/10.1038/nature05058)
- Wu C, Hong L, Ou C (2012) Blood cell-free plasma separated blood samples with a cascading weir-type microfilter using dead-end Filtration. *J Med Biol Eng* 32(3):163–168
- Yang X, Forouzan O, Brown TP, Shevkoplyas SS (2012) Integrated separation of blood plasma from whole blood for microfluidic paper-based analytical devices. *Lab Chip* 12:274